



HAL
open science

Flexure and Seismicity across the Ocean-Continent Transition in the Gulf of Cadiz

Maria C. Neves, Rui G.M. Neves

► **To cite this version:**

Maria C. Neves, Rui G.M. Neves. Flexure and Seismicity across the Ocean-Continent Transition in the Gulf of Cadiz. *Journal of Geodynamics*, 2009, 47 (2-3), pp.119. 10.1016/j.jog.2008.07.002 . hal-00531889

HAL Id: hal-00531889

<https://hal.science/hal-00531889>

Submitted on 4 Nov 2010

HAL is a multi-disciplinary open access archive for the deposit and dissemination of scientific research documents, whether they are published or not. The documents may come from teaching and research institutions in France or abroad, or from public or private research centers.

L'archive ouverte pluridisciplinaire **HAL**, est destinée au dépôt et à la diffusion de documents scientifiques de niveau recherche, publiés ou non, émanant des établissements d'enseignement et de recherche français ou étrangers, des laboratoires publics ou privés.

Accepted Manuscript

Title: Flexure and Seismicity across the Ocean-Continent
Transition in the Gulf of Cadiz

Authors: Maria C. Neves, Rui G.M. Neves

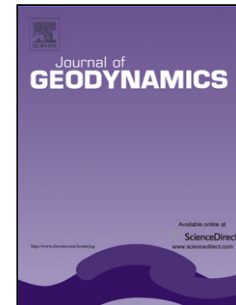
PII: S0264-3707(08)00061-6
DOI: doi:10.1016/j.jog.2008.07.002
Reference: GEOD 858

To appear in: *Journal of Geodynamics*

Received date: 8-11-2007
Revised date: 30-6-2008
Accepted date: 15-7-2008

Please cite this article as: Neves, M.C., Neves, R.G.M., Flexure and Seismicity across the Ocean-Continent Transition in the Gulf of Cadiz, *Journal of Geodynamics* (2007), doi:10.1016/j.jog.2008.07.002

This is a PDF file of an unedited manuscript that has been accepted for publication. As a service to our customers we are providing this early version of the manuscript. The manuscript will undergo copyediting, typesetting, and review of the resulting proof before it is published in its final form. Please note that during the production process errors may be discovered which could affect the content, and all legal disclaimers that apply to the journal pertain.



1

2 **Flexure and Seismicity across the Ocean-Continent Transition in the Gulf**
3 **of Cadiz**

4

5 Maria C. Neves^{1,*} and Rui G.M. Neves²

6

7 ¹ CIMA-FCMA, Universidade do Algarve, Campus de Gambelas, 8000 Faro, Portugal

8 ² UIED-FCT, Universidade Nova de Lisboa, Monte da Caparica, 2829 Caparica, Portugal

9

10 *Corresponding author: Tel: +351 289800938; fax: +351 289800069 E-mail address:

11 mneves@ualg.pt (M.C. Neves)

12

13 **Abstract**

14

15 In the Gulf of Cadiz the water/sediment load and the density contrasts between the
16 continental and oceanic lithosphere are sources of vertical loading causing flexure. The
17 main objective of this work is to investigate the relation between the bending stresses
18 associated with flexural isostasy and the observed pattern of deformation and seismicity.
19 For that we combine a strength analysis and finite element numerical modelling along a
20 previously studied (Fernandez et al., 2004) vertical section of the lithosphere,
21 approximately perpendicular to the Africa-Eurasia convergence. We find that the flexural
22 stresses are focussed in the ocean-continent transition, within a zone approximately 150 km
23 wide, between the base of the continental slope and the Horseshoe Abyssal Plain. We show

24 that the flexural stresses are mainly supported by the upper mantle and predict their values
25 for two different thermal scenarios. The compositional layering in the crust is shown to
26 play an important role in the focussing of the strain energy along the crust/mantle interface.
27 Finally, we observe that there is a correlation between the modelled strain energy and the
28 earthquake distribution. The maximum compressive stress difference can be as much as
29 65% of the strength in compression. The maximum influence is observed at 10 km depth
30 near the Horseshoe Abyssal Plain. We conclude that flexural stresses alone are not enough
31 to cause rupture or yielding in the Gulf of Cadiz. However, like plate boundary forces and
32 inherited mechanical weaknesses, they need to be incorporated when assessing seismic
33 hazard in this region.

34

35 Keywords: Flexure; strength; ocean-continent transition; seismicity; Gulf of Cadiz.

36

37

38 **1. Introduction**

39

40 The Gulf of Cadiz, including the Algarve continental margin and the seaward continuation
41 of the Guadalquivir Basin, frames the Africa-Eurasia plate boundary to the west of the
42 Gibraltar Strait (Figure 1). Its structure is the result of a complex evolution involving
43 several processes (e.g. Gràcia et al., 2003): (1) extensional processes related to Pangea
44 rifting and Atlantic opening which led to the creation of a passive margin in the western
45 part of the Gulf; (2) convergence between the African and Eurasian plates that, since the
46 Oligocene, dominates the structural and tectonic setting; and (3) the westward movement of

47 the Alboran domain during the Miocene, responsible for the Betics and the Guadalquivir
48 foreland basin, which caused the emplacement of allochthonous terrains.
49
50 In process (1), rifting along the southern Iberian margin started approximately in the Early
51 Jurassic (190Ma) resulting in the break-up of a previously existing large carbonate and
52 clastic shelf (e.g. Andeweg, 2002). Active rifting changed to post-rift during the Late
53 Jurassic (160Ma) with related thermal subsidence lasting until the Cretaceous (Vera, 1988
54 in Andeweg, 2002). The early evolution of the margin and the limits of the oceanic and
55 continental domains in the Gulf of Cadiz remain unclear. Wide-angle and seismic reflection
56 data, as well as gravity data, indicate a continental domain beneath the central Gulf of
57 Cadiz, with Moho depths varying between ~30 km near the coastline to ~20 km offshore,
58 and an oceanic domain in the region of the Horseshoe Abyssal Plain, with Moho depths of
59 ~12 km (e.g. Purdy, 1975; González-Fernández et al., 2001; Fernandez et al., 2004).
60 However, the location of the ocean-continent transition is controversial, with some authors
61 arguing that a portion of oceanic lithosphere, formed during the Tethys opening, is still
62 present in a presumed fore arc region in the central part of the Gulf (e.g. Maldonado et al.,
63 1999; Gutscher et al., 2002). In the cross section of the lithosphere we consider in this
64 study, the ocean-continent transition occurs in the contact area between transition zones 1
65 and 2 in Figure 1.
66
67 Process (2), the convergence between the Africa and the Eurasia plates, has been one of the
68 most important sources of stress not only in the Gulf of Cadiz but also all over Iberia
69 (Andeweg, 2002). Large-scale lithosphere and upper crustal folding distributed across
70 Iberia, with dominant wavelengths of ~250 km and ~50 km, has been shown to have

71 resulted from shortening at both the northern and southern margins of Iberia (Cloetingh et
72 al., 2002). The plate kinematics computed from GPS data shows that present-day Africa-
73 Eurasia convergence occurs in a NW-SE to WNW-ESE direction at a rate of approximately
74 4-5 mm/yr (e.g. Fernandes et al., 2003; Nocquet and Calais, 2004; Fernandes et al., 2007).
75 In the Gulf of Cadiz this convergence is essentially accommodated by diffuse brittle
76 deformation as evidenced by widely developed tectonic structures, with different
77 orientations and kinematics: predominantly NNE-SSW striking thrusts and WNW/ESE
78 trending dextral strike-slip faults (e.g. Gràcia et al., 2003; Sartori et al., 1994; Pinheiro et
79 al., 1996; Hayward et al., 1999; Zitellini et al., 2001; Zittelini et al., 2004; Terrinha et al.,
80 2003; Medialdea et al., 2004). Other evidence of this diffuse brittle deformation is the
81 seismicity in the area. Earthquake epicentres are mainly limited to an E-W trending area
82 about 150 km wide and ranging from 7°W to 12°W (Figure 1). Most earthquakes occur at
83 depths less than 150 km (e.g. Bufforn et al., 2004). Large events occur at shallow depths (<
84 30 km) and show thrust and strike-slip faulting mechanisms consistent with the
85 predominant NNE-SSW and WNW-ESE fault directions under the observed NW-SE
86 convergence direction (e.g. Stich et al., 2006).

87

88 The dominance of the evidence of compression may explain why flexural effects have so
89 far been neglected in the offshore region. Inland, flexural isostasy plays a major role,
90 particularly in the Guadalquivir Basin, whose origin is explained by an elastic plate model
91 loaded both on top by topography and from below by crustal and lithospheric mantle
92 thickness variations (Van der Beek and Cloetingh, 1992). Further flexural modelling of
93 the evolution of this basin emphasized the role of rheological layering and pointed to the

94 importance of viscous stress relaxation and/or plastic yielding within the lithosphere
95 (Garcia-Castelhanos et al., 2002). Offshore the Algarve margin, flexural effects may also
96 arise due to the lateral density variations created by the co-existence of the oceanic and
97 continental domains.

98
99 However, previous numerical models in the Gulf of Cadiz have ignored the strength of the
100 lithosphere and assumed local isostatic equilibrium. This assumption was made in the study
101 by Fernandez et al. (2004) who used a finite element code to solve simultaneously the
102 geopotential, lithostatic and heat transport equations to estimate the rock parameters and
103 thermal properties of the lithosphere along a profile across the ocean-continent transition. It
104 was also made by Jimenez-Munt et al. (2001) and Negredo et al. (2002) who used the thin
105 sheet approach to provide first order approximations of the strain and strain rate distribution
106 in the Gulf of Cadiz. These efforts allowed the testing of hypotheses about kinematic poles
107 and boundary conditions and provided indications on the long-term seismic hazard of faults
108 by estimating their fault slip rates. Nevertheless, this 2D horizontal approach cannot resolve
109 vertical variations of strength and neglects flexural stresses.

110
111 In this work we aim to address these issues. Our main goals are threefold: (1) provide an
112 estimate of the bending stresses and assess how important flexural isostasy may be in the
113 Gulf of Cadiz; for this we model the Fernandez et al. (2004) vertical profile cutting across
114 the continental and oceanic domains; (2) investigate the role of a layered rheology in the
115 stress distribution; for this we use the crustal structure documented by Fernandez et al.
116 (2004) to infer the vertical strength variations along the same profile and estimate the
117 mechanical thickness in this region; and (3) explore the relation between the bending

118 stresses and the seismicity. Recognising that the bending stresses induced by flexural
119 loading might be one of the possible causes of earthquakes (e.g. Watts, 2001), we combine
120 the strength analysis with the numerical modelling to investigate the relation between
121 flexure and the observed pattern of deformation and seismicity.

122

123 **2. Crustal Structure**

124

125 The lithospheric structure in the Gulf of Cadiz has been the subject of numerous seismic
126 campaigns justified in part by the seismic hazard risk in this region. In addition to the
127 seismic reflection profiles of the oil industry, many near-vertical reflection, refraction and
128 wide-angle reflection profiles have been acquired in recent years within the scope of
129 projects such as RIFANO92, IAM93, BIGSETS98, TASYO-2000, SISMAR2001 and
130 VOLTAIRE2002. Among these projects IAM93 was pioneer in revealing the deep structure
131 of the crust and mantle (Banda et al., 1995). The combined interpretation of near-vertical
132 reflection and refraction/wide-angle reflection IAM data first suggested that the crust
133 underlying the eastern and central part of the Gulf of Cadiz is of continental type, with a
134 continental basement formed by Precambrian and Palaeozoic rocks (González-Fernández et
135 al., 2001). The Moho gradually shallows from a depth of 30-32 km in the continental
136 margin of SW Iberia to 10-12 km in the Horseshoe Abyssal Plain (HAP), reaching values
137 of less than 7 km in the Seine Abyssal Plain (SAP) (Purdy, 1975; Sartori et al., 1994;
138 Matias, 1996; González et al, 1998). The oceanic nature of the crust in the HAP, the SAP
139 and in the Gorringe Bank is generally accepted on the grounds of seismic interpretation,
140 gravity anomaly modelling and bottom sampling (e.g. Purdy, 1975; Hayward et al., 1999;

141 Gràcia et al., 2003). In the region between the continental domain of the Gulf of Cadiz and
142 the oceanic domain of the HAP there is no clear evidence of crust type.

143

144 The section of the lithosphere considered in this study is represented in Figure 2. Between
145 the eastern end of the HAP and Cape San Vincent (CSV) it coincides with seismic
146 reflection profile IAM3, already studied in great detail by several authors (e.g. Gonzalez et
147 al., 1996; Tortella et al., 1997). In the SAP the crustal structure is based on the work of
148 Purdy (1975), Sartori et al. (1994) and Medialdea et al. (2004). Inland of CSV, in the South
149 Portuguese Zone, it is based on the interpretation of seismic wide-angle and refraction data
150 by Matias (1996) and González et al. (1998). Rather than strictly following the seismically
151 defined interfaces, we incorporate the results of the modelling of Fernandez et al. (2004) to
152 define the geometry and physical properties of the different layers.

153

154 Regarding the basement, four main zones can be identified along the section of Figure 2.
155 From SW to NE: (1) an oceanic domain around the SAP where the crust, about 7 km thick,
156 is divided into an upper part with P-wave velocities in the range 4.1-5.6 km/s and a lower
157 part with velocities of about 6.3 km/s; (2) a transitional domain spanning from around km-
158 300 to km-150 where the crust has an intermediate composition/density between that of
159 oceanic crust/2840 kg/m³ and that of upper continental crust/2740 kg/m³; (3) a second
160 transitional domain ranging from km-150 km to km-50 consisting of stretched continental
161 lithosphere. This domain consists of two layers with seismic velocities analogous to the
162 upper and middle continental crust; (4) a continental crust characterized by three layers that
163 thickens to 30 km within 50 km of CSV. Here P-wave velocities are 5.2-6.1 km/s in the
164 upper crust, 6.2-6.4 km/s in the middle crust, 6.7-6.9 km/s in the lower crust and 8.1-8.2

165 km/s in the mantle. We call the ocean-continent transition the region near km-150 lying
166 between transitional zones 1 and 2.

167

168 The sedimentary cover is continuous from the SAP to CSV having a variable thickness that
169 reaches its maximum (~ 2 s TWT) in the eastern HAP. It consists of five stratigraphic units,
170 spanning in age from upper Jurassic-lower Aptian at the base to Miocene-Quaternary at the
171 top (Tortella et al., 1997; Medialdea et al., 2004). Among these units the allochthonous
172 body of the Gulf of Cadiz, about 400-500 ms TWT thick in the HAP, is particularly
173 relevant for its chaotic character and role in the geodynamic evolution of this region. P-
174 wave velocities in the depositional sequence range from 2.0 km/s in the post-Miocene
175 marine sediments at the top to 3.7 km/s in what is interpreted as the Mesozoic carbonate
176 succession also found in the Algarve margin outcrops.

177

178 The SAP and the HAP are characterised by active thrust tectonics, with a northwestward
179 verging thrust system trending NNE-SSW affecting both the sediment cover and the
180 basement. Some of these thrust faults are observed as internal crustal reflectors that sole out
181 developing seafloor elevations (e.g. Terrinha et al., 2003; Medialdea et al., 2004).

182 Shortening in the region is also expressed as large amplitude (up to 800 m) and
183 intermediate wavelength (10-60 km) folds of the sediments and basement (Hayward et al.,
184 1999; Medialdea et al., 2004). Similar intermediate wavelength folds are also observed
185 within the Iberia Peninsula (Cloetingh et al., 2002). The NNE-SSW thrust system is
186 crosscut by lineaments trending WNW-ESE that have been interpreted as seafloor
187 manifestations of deep right-lateral strike-slip faults (Terrinha et al., submitted).

188

189 3. Seismicity

190

191 The seismicity data used in this study is taken from the IM Seismic Catalogue of
192 Continental Portugal and adjacent region for 1970-2000, and from the ISC catalogue
193 (<http://www.isc.ac.uk/Bulletin>) for the period from 1964 to the present. As shown in Figure
194 1 the seismicity from 12° W to 7° W is distributed in an E-W direction within a band of
195 approximately 150 km. Within this band three regions of concentrated events, which seem
196 to be SW-NE oriented, can be recognised: the region of the Gorringe Bank, the region that
197 runs from CSV along the S. Vicente Canyon to the HAP, and the region of the
198 Guadalquivir Bank. The largest events concentrate in the HAP (29.2.1969, Ms=8 and
199 12.2.2007, Mw=6.1) but the majority have small to moderate magnitudes (Ms < 5).

200

201 Earthquakes are observed up to 140 km depth both in the oceanic and continental domains
202 (e.g. Bufoin et al., 2004). In the oceanic lithosphere the brittle-ductile transition often
203 occurs in the mantle so the depths of the events recorded to the west of 10° W are
204 considered normal. In the region to the east of this longitude the explanation for the
205 observed intermediate-depth seismicity is more controversial since the continental mantle is
206 generally aseismic at these depths.

207

208 Focal mechanisms show essentially thrust and strike-slip faulting, with thrusting motion
209 dominating (e.g. Udías et al., 1976; Grimison and Chen, 1986; Borges et al., 2001; Bufoin
210 et al., 2004). The strike-slip solutions have predominantly E-W striking planes with right-
211 lateral motion. The seismicity studies are unanimous in considering that both thrust and

212 strike slip events are compatible with a NNW-SSE direction of horizontal maximum of
213 compression (σ_1), close to the direction of the plate convergence between Africa and
214 Eurasia. Furthermore, both the shallow and deep earthquakes show the same direction of
215 maximum compression, supporting the hypothesis of mechanical crust-mantle coupling
216 (Stich et al., 2006). There is nonetheless some evidence that the least compressive stress is
217 steeper at the surface and more sub-horizontal at depth, suggesting a transition in the
218 faulting regime from reverse faulting at shallow depths to strike-slip faulting at
219 intermediate depths (Stich et al., 2006).

220

221 Figure 3 shows a cross section of the seismicity along the profile considered in this study.
222 All projected earthquakes lie in a 150 km wide band centred on the profile thus excluding
223 events in the Gorringe Bank and in the Guadalquivir Bank. Alignments of earthquakes at
224 10 and 30 km depth have been filtered out from the IM database as these correspond to
225 poorly constrained hypocenters (F. Carrilho, personal communication). The geometry of
226 the crust is shown in the background for reference, but note that the vertical axis in Figure 3
227 represents depth below the seafloor and not depth below sea level as in Figure 2.

228

229 Looking at Figure 3 we can divide the seismicity into four main zones: (1) a practically
230 aseismic oceanic domain; (2) a transitional domain called “transition 2” dominated by the
231 cluster of relatively larger earthquakes in the HAP extending from km-250 to km-150; (3)
232 another transition zone called “transition 1”, from km-150 to km-50, marked by the cluster
233 of small magnitude events near the base of the crust running along San Vincent Canyon.
234 Their alignment suggests the presence of a fault plane sub-parallel to the base of the crust;
235 and finally (4) a continental domain characterised by small magnitude earthquakes mostly

236 confined within the crust. The presence of a local short-period seismic network since 1996
 237 near Monchique contributed to the high density of recorded events near km-50 (Carrilho et
 238 al., 2004). Relatively larger events ($M_L > 4$) occur at the top of the crust and in the upper
 239 mantle beneath the continental shelf. These events have known fault plane solutions
 240 showing a dominant strike-slip faulting regime. Extension parallel to the steepest
 241 topography due to lateral density variations can facilitate the strike slip regime here, i.e.
 242 modify pure compression to strike slip (Andeweg, 2002).

243

244 **4. Rheology**

245

246 **4.1 Deformation laws**

247

248 To constrain the mechanical structure of the lithosphere in the Gulf of Cadiz we use the
 249 concept of yield strength envelope. This concept is based on the assumption that at low
 250 confining pressures and temperatures fracturing is predominant, while at high temperatures
 251 creep deformation mechanisms dominate in the lithosphere. For the brittle regime the
 252 critical stress difference at failure (the yield strength) is given by the Coulomb frictional
 253 law, assuming faults of favourable orientation and negligible cohesion (Sibson, 1974),

254

$$255 \quad \sigma_1 - \sigma_3 = \alpha \rho g z (1 - \lambda) \quad (\text{Eq. 1})$$

256

257 where $\sigma_1 - \sigma_3$ is the maximum stress difference, α is a constant related to the fault type and
 258 frictional coefficient, ρ is the average density of rocks above depth z , and λ is the pore fluid

259 factor. In the absence of information regarding the pore fluid factor we assume hydrostatic
 260 conditions ($\lambda=0.4$). A friction coefficient of 0.75 common for most rock types gives $\alpha=3.0$
 261 in compression (thrust faulting) and $\alpha=0.75$ in extension (normal faulting).

262

263 In the ductile regime, deformation is assumed to follow a power-law dislocation creep
 264 equation (Ranalli, 1995),

265

$$266 \quad \sigma_1 - \sigma_3 = \left(\frac{\dot{\epsilon}}{B} \right)^{\frac{1}{n}} \exp\left(\frac{A}{nRT} \right) \quad (\text{Eq. 2})$$

267

268 where $\dot{\epsilon}$ is the strain rate (s^{-1}), R is the universal ideal gas constant, T is the absolute
 269 temperature, A is the creep activation enthalpy and B and n are material creep parameters.
 270 The yield strength envelope is built assuming that at each depth the maximum stress
 271 difference is given by the minimum of Eq. (1) and (2). We further assume, as a first-order
 272 approximation, that the brittle-ductile transition is sharp.

273

274 We also assume that the present-day bulk strain rate is 10^{-16} s^{-1} . This is an average value
 275 consistent with measurements of present-day shortening rates of 4-5 mm/yr (e.g. Fernandes
 276 et al., 2003) averaged over an area of horizontal deformation of about 150 km, and also
 277 with numerical modelling results in the Gulf of Cadiz that include the contribution of both
 278 fault slip and inelastic deformation (Jimenez-Munt et al., 2001; Negrodo et al., 2002).

279

280 The rheological structure along the profile was derived from the density and seismic
281 velocity model (Figure 2) following studies that correlate seismic velocities measured in the
282 laboratory and the dominant lithology (e.g. Christensen and Mooney, 1995; Okaya et al.,
283 1996). Although a unique correlation does not exist, a first order petrological classification
284 derived from seismic P-wave velocities and densities is listed in table 1. Creep parameters
285 for the several rheologies were taken from Afonso and Ranalli (2004).

286

287 The main lithologic units in the continent are quartzite in the upper crust, felsic granulite in
288 the middle crust, mafic granulite in the lower crust and peridotite in the mantle. We have
289 adopted hydrated rheologies because these seem to be appropriate in most continental
290 environments affected by Post-Paleozoic tectono-thermal events (Afonso and Ranalli,
291 2004). For the oceanic crust we assumed the wet diabase deformation law.

292

293 **4.2 Temperature and Strength**

294

295 Estimates of surface heat flow in SW Iberia are scarce. In the South Portuguese Zone the
296 few measurements available range between 60 and 70 mW/ m² (Fernandez et al., 1998), so
297 we assumed a continental surface heat flow of 64 mW/m². Offshore the heat flow is even
298 less constrained with very few available heat flow measurements in the region of the
299 Horseshoe Abyssal Plain (HAP) indicating an average value of 57±15 mW/m² (Fernandez
300 et al., 1998; Verzhbitsky and Zolotarev, 1989). The Fernandez et al. (2004) modelling
301 yielded a value of about 40 mW/m² in the HAP but this value is not consistent with the

302 asymptotic geotherm for oceanic lithosphere more than 120 Ma old. (Hayward et al. (1999)
303 suggested an age of ~152 Ma for the oceanic lithosphere in the nearby Gorringe Bank.)

304

305 Given the scarcity of surface heat flow measurements we reconstructed the temperature
306 structure along the modelled profile by fixing 5 geotherms (GT1 to GT5) and linearly
307 interpolating between them (Figure 4a). GT4 (=GT5) is the asymptotic geotherm for oceanic
308 lithosphere 120 Ma old, computed according to the Plate Cooling Model (mantle
309 temperature = 1330°C and plate thickness = 125 km). In the transition zones and in the
310 continental margin the geotherms were computed by solving the steady state 1-D heat
311 conduction equation with radiogenic heat production for three-layer lithospheric models of
312 varying thickness and composition. For GT3 at km -150 the three layers considered were
313 sediments, crust (UC+MC average, see figure 2) and mantle. For GT2 and GT1 we used the
314 upper crust, the combined mid- and lower crust (MC+LC), and mantle. Note that the
315 sediments are included in the thermal structure computation for their blanketing effect but
316 they are stripped off the numerical model (section 5). The heat production rates and thermal
317 conductivities for the several rock compositions are listed in Table 1 and were taken from
318 Afonso and Ranalli (2004).

319

320 The present-day strength envelopes for different sites along the profile are shown in Figure
321 4a. We only show the envelopes for compression because this is the dominant regime in the
322 Gulf of Cadiz. An extensional regime, which can exist locally, would produce slightly
323 deeper cut-off depths of brittle strength. In the continent there is mechanical layering with
324 ductile layers in the crust, particularly at the bottom of the middle (felsic granulite) and

325 lower (mafic granulite) crust. In contrast, there are no ductile interleaved layers in the
326 transition and oceanic zones. There, the upper-crust strength is essentially in the brittle
327 domain with a slight deepening of the brittle-ductile transition oceanwards. However, most
328 of the strength resides in the mantle and there are no pronounced lateral strength variations.
329 These are general features that remain unchanged when other sensible composition options
330 are considered.

331

332 The rheological structure adopted to construct the strength envelope is not free from
333 ambiguities (e.g. Ranalli, 2003; Burov, 2003). To address the effect of another temperature
334 structure on the strength-depth distribution we considered the hypothetical scenario shown
335 in Figure 4b. A cosine bell function was used to interpolate between geotherms T1 and T2
336 (Figure 4b), inspired on the work of Cowie et al. (2005) who used a similar procedure. T1
337 is the continental geotherm computed as in figure 4a assuming a continental surface heat
338 flow of 64 mW/m^2 and a surface temperature of 15°C . T2 is the geotherm for oceanic
339 lithosphere 10 Ma old computed according to the Plate Cooling Model. Taking into account
340 that the age of the oceanic lithosphere at the end of the rifting in the western part of the
341 Gulf of Cadiz was 30 Ma, the thermal structure in Figure 4b may perhaps resemble that of
342 the active rifting stage. To isolate the effect of the temperature we assumed a present-day
343 composition and strain rate. In this hypothetical scenario the cut-off depth of the brittle
344 strength shallows oceanwards producing a significant reduction of strength in the transition
345 and oceanic zones (Figure 4b). Nevertheless, the strength in the transitional and oceanic
346 zones still resides mostly in the mantle.

347

348 **5. Flexural modelling**

349

350 Vertical loads in isostatic equilibrium produce flexure and bending when the lithosphere
351 has non-zero strength. However, the importance of flexural isostasy to the overall
352 deformation has not been duly emphasised in previous studies of the Gulf of Cadiz. To
353 address this problem we used an elasto-visco-plastic 2D finite element modelling approach
354 and analysed the deformation in terms of stress and strain distribution with depth.

355

356 **5.1 Numerical procedure**

357

358 To perform the elasto-plastic simulations we used a modified version of the FEVPLIB
359 finite element program that was described in detail by Bott (1997). This package
360 incorporates elasto-plastic deformation with a finite yield strength using the viscoplastic
361 method and has been used to model stress and displacements produced by anomalous
362 density in a variety of tectonic settings (e.g. Bott, 1997; Zhang and Bott, 2000; Neves et al.,
363 2004). The yield strength is computed at each depth assuming brittle and power-law creep
364 deformation depending on temperature. The temperature structure is specified as input and
365 the thermal evolution is not modelled. When the yield strength is exceeded, the excess
366 stress is removed using a time stepping scheme. The condition for plastic yielding obeys
367 the Mohr-Coulomb criterion.

368

369 The finite element grid that represents the vertical section of the lithosphere is 600 km long
370 and 140 km deep. Quadrilateral elements with eight nodes form a regular grid with
371 maximum resolution of 1 km x 0.5 km in the topmost 30 km. The plane strain hypothesis,
372 suitable to study flexure in two-dimensions, is assumed. As boundary conditions we fix the

373 SW end of the model in the horizontal direction, but let it be free to move in the vertical
374 direction. Other boundaries are free to move in both directions. Isostatic boundary
375 conditions are applied at the surface to simulate isostatic restoring forces.

376

377 **5.2 Applied loads**

378

379 The development of topography is the flexural isostatic response of the model to the
380 vertical loads. The vertical loads are separated in two parts: (1) the weight of the sediments
381 and water and (2) the gravitational body forces due to the lateral density contrasts caused
382 by continental stretching.

383

384 The sediment and water load is applied instantaneously as direct nodal forces
385 (Figure 5a). The seawater and sediment layers are removed and all density interfaces lying
386 underneath shifted upwards, so that the top of the basement is initially at the surface of the
387 finite element model (Figure 5b). The gravitational body forces are incorporated as density
388 anomalies relative to a reference density-depth profile at the SW end of the model. The
389 reference density-depth profile comprises two layers: normal oceanic crust 7 km thick and
390 uniform mantle below, with densities of 2840 and 3300 kg/m³, respectively. The density
391 anomalies are obtained by subtracting the reference depth-density profile from the density
392 structure (Figure 5c). Negative density anomalies generate buoyancy forces and uplift,
393 while positive anomalies generate downward forces and subsidence. While the sediment
394 and water load produce concave upward flexure, buoyancy of the continental crust relative
395 to the oceanic crust/mantle causes the uplift of the continental margin relative to the ocean
396 basin (Figure 6).

397

398 **5.3 Modelling Results**

399

400 The loads in Figure 5 have been applied to the two strength-depth distributions shown in
401 Figure 4. The resulting flexural response of the lithosphere is now examined in terms of the
402 patterns of differential stress and strain energy. The relation of these with the observed
403 seismicity is discussed in the next section. The differential stress is the difference between
404 the horizontal and vertical stress in the vertical plane of the model. The conditions for
405 failure can be described using this difference. According to Anderson's theory of faulting
406 and following Sibson (1974) the faulting regimes can be classified as normal or as thrust if
407 the maximum compressive stress is vertical or horizontal, respectively. Since the plane
408 strain formulation implies that the out-of-plane stress is the intermediate stress, our models
409 foresee a normal or thrust fault regime depending on the sign and magnitude of the
410 differential stress. We use the convention that a negative differential stress corresponds to
411 compression (thrust fault regime) and a positive differential stress to an extension (normal
412 fault regime). The density of the strain energy (strain energy per unit of volume hereafter
413 shortly called strain energy) is the energy contained in a material as a consequence of its
414 elastic deformation (Ranalli, 1995). The strain energy state, and its variations with time,
415 reflect the intensity of crustal activity and is an important index of earthquake potential.

416

417 The differential stress and strain energy due to flexure are shown in Figure 7 for the actual
418 and hypothetical scenarios. The pattern of differential stress reflects the downward
419 deflection of the lithosphere and is typical of concave elastic bending: negative stresses

420 occur at relatively shallow levels due to contraction and positive values occur at the bottom
421 due to extension. Vertically, the largest stresses concentrate at a depth of approximately 10-
422 40 km in the hypothetical scenario and at 10-50 km in the actual state. This depth range
423 corresponds to the elastic core that is capable of supporting flexural stresses on a long time
424 scale. Laterally, the largest differential stresses occur where the plate curvature reaches its
425 maximum, between km-200 and km-50. Moreover, there is no significant propagation of
426 stresses seawards or landwards, that is, the effect of bending is rather localized in the
427 transition zone. The compressive stresses focus just below the base of the crust regardless
428 of the temperature structure, although they spread over a wider area in the actual state. In
429 contrast, the trend of the region of extension, dipping to the NE in the hypothetical
430 scenario, is controlled by the lateral temperature gradient.

431

432 The pattern of strain energy is very similar to that of the differential stress being distributed
433 into approximately two main areas. Comparing the two scenarios the upper area, adjacent
434 to the Moho, remains nearly stationary, while the lower area is deduced to deepen and
435 rotate towards the horizontal in the actual state. The release of the strain energy in the form
436 of earthquakes is more likely to occur in regions where the strain energy accumulates. The
437 strain energy accumulates in the upper mantle and not in the crust. Thus, the Moho limits
438 the upper strain accumulation region. This strong dependence of strain energy on
439 composition is even more evident in Figure 8. The strain pattern produced by a uniform
440 crust model (top) is quite different from that produced by a more realistic model that
441 includes compositional layering in the crust (bottom). This result shows that a layered
442 rheology seems to be more at its place in this situation.

443

444 **6. Discussion**

445

446 **6.1 Flexure and earthquakes**

447

448 The time scale of seismic energy release is certainly different from the time scale of elastic
449 plate flexure. So, it is extraordinary to observe a correlation between estimates of elastic
450 plate thickness and estimates of seismogenic layer thickness. Indeed, in the Pacific Ocean
451 the earthquakes show a distribution and a focal mechanism pattern that seems to be directly
452 connected to the up-warping of the oceanic lithosphere seaward deep-sea trenches (e.g.
453 Watts, 2001; Tassara et al., 2007). In the continents this relation is harder to prove and has
454 been strongly debated (e.g. Maggi et al., 2000; Watts and Burov, 2003; Handy and Brun,
455 2004). One of the reasons for such difficulty is that the continents have been subjected to
456 more complex evolution histories than the oceans. In addition, the lithosphere's "memory"
457 justifies the existence of earthquakes which are related with the sequence of geological
458 processes and not with the actual deformation state (e.g. Mueller et al., 1996).

459

460 It is obvious that flexure is not the only source of stress in the Gulf of Cadiz. Geological,
461 geodetic and focal mechanism data show that the region is dominated by NW-SE
462 compression associated with the Africa-Eurasia convergence. Moreover, inherited
463 mechanical weaknesses are certainly a key factor in the distribution of stress. It is therefore
464 expected that the earthquakes are releasing energy of deformation associated with the plate
465 convergence, focussed at inherited mechanical weaknesses. So the question is whether or
466 not flexure contributes to the actual state of stress. In our opinion figure 7 shows that there
467 is a clear correlation between strain energy associated with flexure and the earthquake

468 distribution. Furthermore, it shows that there is a relation between seismicity and
469 mechanical discontinuities connecting zones of contrasting density and rheology. This
470 relation is particularly visible in the upper mantle just below the Moho between km-110
471 and km-70. Another correlation between the modelling results and the seismicity is the
472 apparent dipping trend to the NE of the distributions along the transition zone. This trend is
473 not only suggested by the cluster of small magnitude events below the Moho but also by
474 the larger magnitude earthquakes with known focal mechanism solutions which become
475 deeper towards the NE (e.g. between km-200 and km-100). This suggests that the strain
476 energy induced by flexure in the past may have created preferential regions of weakness,
477 which are now being reactivated in the actual state of compression.

478

479 It is evident that there are other clusters of events, particularly in the continental region,
480 which do not show any correlation with flexure. These events may be due to other local
481 processes and/or may be related to the 3D nature of the deformation. For instance, the
482 lateral density variations associated with the changing trend of steep topographic slopes,
483 from nearly EW along the Algarve coast to NS north of the Gorringe bank, can lead to
484 extensional and strike slip deformation under predominantly pure compressional
485 deformation (Andeweg, 2002). These hypotheses need further investigation using a full 3D
486 modelling approach that is currently under way. 3D modelling will also allow us to explore
487 the relation between the focal mechanisms and the strain/stress-depth distribution.

488

489 **6.2 The strength of the Ocean-Continent Transition**

490

491 It has long been recognised that Ocean-Continent Transition zones are often weak relative
492 to normal oceanic and continental lithosphere. This is expressed by low values of elastic
493 plate thickness in extended continental lithosphere, reflecting a long-term mechanical
494 weakness (e.g. Watts and Stewart, 1998). The reasons behind such a weak behaviour on
495 long-time scales are still unclear. When the beta stretching factor is greater than 3, models
496 of extension at the West Iberia margin predict embrittlement of the whole crust with
497 development of crustal penetrating faults which can act as fluid conduits, allowing
498 serpentinization of the upper mantle peridotites (Pérez-Gussinyé and Reston, 2001). The
499 coefficient of friction of serpentinite (~0.3) is considerably lower than that predicted by
500 Byerlee's law (Escartin et al., 1997). Moreover, serpentinites may favour the confinement
501 of fluids within fault zones, contributing to an increase in the pore fluid factor and to a
502 strength reduction of the whole crust. This would partially explain the concentration of
503 deformation and seismicity in ocean-continent transition zones subjected to large present-
504 day tectonic stresses.

505

506 In this study we have not incorporated any weakness in the transition zone, since we have
507 used a constant coefficient of friction of 0.75 to build the brittle part of the strength
508 envelope. Consequently, the integrated strength is predicted to increase gently along the
509 profile, from 3.2×10^{13} N/m in the continent (km-50) to 4.4×10^{13} N/m in the ocean (km-
510 250) (Figure 9). The mechanical thickness of the lithosphere (depth above which the
511 strength > 10 MPa) is 48 and 45 km in the oceanic and transition zones respectively.

512

513 Only in the case of a single-layer elastic rheology, high flexural rigidity and small
514 curvatures will the elastic thickness approach the mechanical thickness (Watts and Burov,

515 2003). Otherwise, the mechanical thickness provides an upper bound limit for the elastic
516 thickness. Thus, in the oceanic lithosphere of the Gorringe Bank, Hayward et al. (1999)
517 found that the gravity anomaly is explained by a discontinuous (broken) elastic plate model
518 35 km thick at the time of loading (the lithosphere would have been 140 Ma old when it
519 was loaded 12 Ma ago). Flexural modelling results in the Western Iberia margin also
520 indicate a present-day elastic layer thickness in excess of 35 km (T. Cunha, personal
521 communication). Yielding related to the Africa-Eurasia convergence and the presence of
522 mechanical weaknesses not considered in this study may therefore explain the discrepancy
523 between the elastic thickness and mechanical thickness estimates in this region.

524

525 According to our results the flexural bending stresses are not enough to cause yielding and
526 reduce the effective elastic thickness. We compare the stress difference in the actual state
527 (Figure 7) and the strength envelope at km-150 and km-50 in Figure 9. The maximum
528 compressive stress difference generated by flexure, which occurs at the base of the crust at
529 km-150, attains 65 % of the strength in compression at the same depth (~10 km). Unless
530 there is a reduction of the brittle strength in the ocean-continent transition, flexure alone is
531 not sufficient to produce brittle failure and earthquakes in the crust and upper mantle.
532 However, its contribution to the overall stress in the Gulf of Cadiz cannot be disregarded.

533

534 **7. Conclusions**

535

536 In the Gulf of Cadiz the density contrast between oceanic and continental crust is a source
537 of vertical loading at the ocean-continent transition. Vertical loads in isostatic equilibrium
538 produce flexure when the lithosphere has non-zero strength. We modelled the flexure on a

539 vertical section of the lithosphere approximately perpendicular to the Africa-Eurasia
540 convergence. Although this approach does not incorporate out-of-plane displacement of
541 material, it allowed us to analyse the contribution of the flexure separately from other
542 sources of stress such as the dominant NW-SE compression. Our main objective was to
543 explore how the bending stresses were related to the observed deformation, especially as
544 regards the actual release of strain energy in the form of earthquakes. Since the strength is
545 an input of the modelling, we have also placed constraints on the mechanical structure of
546 the lithosphere. The main conclusions of our study are thus the following:

547

- 548 • The flexural stresses are focussed in the ocean-continent transition, within a ~150
549 km wide zone between km-250 and km-50 of the modelled profile.
- 550
- 551 • The focussing of bending stresses on the transition zone is predicted for different
552 thermal scenarios so this result is relatively independent of temperature.
- 553
- 554 • The bending stresses are mainly supported by the upper mantle and show a bipolar
555 distribution. The compressive stresses concentrate just below the Moho (at ~10 km
556 depth in the ocean-continent transition). The tensile stresses underneath (at ~40 km
557 depth) show a dipping trend that is controlled by the lateral temperature gradient.
- 558
- 559 • The strain energy due to flexure also resides in the upper mantle. The largest
560 accumulation of strain energy occurs below the stretched continental lithosphere
561 underneath the Moho. Near km-100 the strain energy concentration coincides with

562 an important cluster of earthquakes located between the S. Vincent fault and the
563 Horseshoe fault.

564

565 • The observed correlation between the strain energy and the earthquake distribution
566 shows that lithospheric flexure exerts a significant control on the seismicity pattern.

567

568 • The compositional layering in the crust plays an important role in the focussing of
569 the strain energy along the crust/mantle interface.

570

571 • Flexural stresses alone are not enough to cause rupture or yielding in the Gulf of
572 Cadiz. However, like plate boundary forces and inherited mechanical weaknesses,
573 they need to be taken into account in the seismic hazard assessment.

574

575 **Acknowledgements**

576

577 We would like to thank Luís Matias, Mourad Bezzeghoud, Fernando Carrilho, Tiago Cunha
578 and Filipe Rosas for useful discussions. We also acknowledge work on free software GMT
579 (Wessel and Smith, 1998) and MIRONE (Luis, 2007). This work is a contribution to the
580 ALMOND project PTDC/CTE-GIN/71862/2006.

581

582 **References**

583

- 584 Afonso, J.C. and G. Ranalli, 2004. Crustal and mantle strengths in continental lithosphere:
585 is the jelly sandwich model obsolete?. *Tectonophysics*, 394, 221-232.
586
- 587 Andeweg, B., 2002. Cenozoic tectonic evolution of the Iberian Peninsula, causes and
588 effects of changing stress fields. PhD thesis, Vrije Universiteit, 178 p.
589
- 590 Banda, E., Torné, M. and I. A. M. Group, 1995. Iberia Atlantic Margin Group investigates
591 deep structure of ocean margins. *Eos Trans. AGU*, 76 (3), 25-29.
592
- 593 Borges, J.F. , Fitas, A., Bezzeghoud, M. and P. Teves-Costa, 2001. Seismotectonics of
594 Portugal and its adjacent area. *Tectonophysics*, 337, 373-387.
595
- 596 Bott, M.H.P., 1997. Modeling the formation of a half graben using realistic upper crustal
597 rheology, *J. Geophys. Res.*, 102, 24605–24617.
598
- 599 Bufforn, E., Bezzeghoud, M., Udías, A. and C. Pro, 2004. Seismic Sources on the Iberia-
600 African Plate Boundary and their Tectonic Implications. *Pure Appl. Geophys.*, 161, 623-
601 646.
602
- 603 Burov, E.B., 2003. The upper crust is softer than dry quartzite. *Tectonophysics*, 361, 321-
604 326.
605

- 606 Carrilho, F., Teves-Costa, P., Morais, I., Pagarete, J. and R. Dias, 2004. Goalgar Project –
607 first results on seismicity and fault plane solutions. *Pure and Appl. Geophys.*, 161 (3), 589-
608 606.
- 609
- 610 Carrilho, F., 2005. Estudo da Sismicidade da Zona Sudoeste de Portugal Continental. Tese
611 de Mestrado em Ciências Geofísicas, Universidade de Lisboa, 160 pp.
- 612
- 613 Christensen, N.I. and W.D. Mooney, 1995. Seismic velocity structure and composition of
614 the continental crust: A global view. *J. Geophys. Res.*, 100 (B7), 9761-9788.
- 615
- 616 Cloetingh, S., Burov, E., Andeweg, B., Beekman, F., Andriessen, P.A.M., Garcia-
617 Castellanos, D., De Vicente, G. and R. Vegas, 2002. Lithospheric Folding in Iberia.
618 *Tectonics*, 21 (5), 5-1.
- 619
- 620 Cowie, P.A., Underhill, J.R., Behn, M.D., Lin, J. and C.E. Gill, 2005. Spatio-temporal
621 evolution of strain accumulation from multi-scale observations of Late Jurassic rifting in
622 the northern North Sea: A critical test of models for lithospheric extension. *Earth and*
623 *Planet. Sci. Lett.*, 234, 401-419.
- 624
- 625 Dañobeitia, J. J., Canales, J.P. and G. A. Dehghani, 1994. An estimation of the elastic
626 thickness of the lithosphere in the Canary Archipelago. *Geophys. Res. Lett.*, 21, 2649-2652.
- 627

628 Escartín, J., Hirth, G. and B. Evans, 1997. Effects of serpentization on the lithospheric
629 strength and the style of normal faulting at slow-spreading ridges. *Earth and Planet. Sci.*
630 *Lett.*, 151 (3-4), 181-190.

631

632 Fernandes, R. M. S., Ambrosius, B.A.C., Noomen, R., Bastos, L., Wortel, M.J.R.,
633 Spakman, W. and R. Govers, 2003. The relative motion between Africa and Eurasia as
634 derived from ITRF2000 and GPS data. *Geophys. Res. Lett.*, 30 (16), 1828,
635 doi:10.1029/2003GL017089.

636

637 Fernandes, R.M.S., Miranda, M., Meijninger, M.B.L., Bos, M.S., Noomen, R., Bastos, L.,
638 Ambrosius, B.A.C. and R.E.M. Riva, 2007. Surface velocity field of the Ibero-Maghrebian
639 segment of the Eurasia-Nubia plate boundary. *Geophy. J. Int.*, 169, 315-324.

640

641 Fernandez, M., Marzán, I., Correia, A. and E. Ramalho, 1998. Heat flow, heat production,
642 and lithospheric thermal regime in the Iberian Peninsula. *Tectonophysics*, 291, 29-53.

643

644 Fernandez, M., Marzán, I. and M. Torné, 2004. Lithospheric transition from the Variscan
645 Iberian Massif to the Jurassic oceanic crust of the Central Atlantic. *Tectonophysics*, 386,
646 97-115.

647

648 Garcia-Castellanos, D., Fernandez, M. and M. Torné, 2002. Modeling the evolution of the
649 Guadalquivir foreland basin (southern Spain). *Tectonics*, 21 (3), 10.1029/2001TC001339.

650

- 651 Gómez-Ortiz, D., Tejero, R., Ruiz, J., Babín-Vich, R. and J.M. González-Casado, 2005.
652 Estimating the effective elastic thickness of the lithosphere of the Iberian Peninsula based
653 on multitaper spectral analysis. *Geophys. J. Int.*, 160 (2), 729-735.
654
- 655 González, A., Torné, M., Córdoba, D., Vidal, N., Matias, L.M. and J. Díaz, 1996. Crustal
656 thinning in the Southwestern Iberian margin. *Geophys. Res. Lett.*, 23 (18), 2477-2480.
657
- 658 González, A., Córdoba, D., Vegas, R. and L. M. Matias, 1998. Seismic crustal structure in
659 the southwest of the Iberian Peninsula and the Gulf of Cadiz. *Tectonophysics*, 296, 317- 31.
660
- 661 González-Fernández, A., Córdoba, D., Matias, L.M. and M. Torné, 2001. Seismic crustal
662 structure in the Gulf of Cadiz (SW Iberian Peninsula). *Mar. Geophys. Res.* 22, 207-223.
663
- 664 Gràcia, E., Dañobeitia, J. , Vergés, J. and R. Bartolomé, 2003. Crustal architecture and
665 tectonic evolution of the Gulf of Cadiz (SW Iberian margin) at the convergence of the
666 Eurasian and African plates. *Tectonics*, 22 (4), 1033, doi:10.1029/2001TC901045.
667
- 668 Grimison, N. L. and W. P. Chen, 1986. The Azores-Gibraltar plate boundary: Focal
669 mechanisms, depths of earthquakes and their tectonic implications. *J. Geophys. Res.*, 91,
670 2029-2047.
671
- 672 Gutscher, M. A., Malod, J., Rehault, J.-P. , Contrucci, I., Klingelhoefer, K., Mendes-Victor,
673 L. and W. Spakman, 2002. Evidence for active subduction beneath Gibraltar. *Geology*, 30
674 (12), 1071-1074.

675

676 Handy, M.R. and J.-P. Brun, 2004. Seismicity, structure and strength of the continental
677 lithosphere. *Earth Planet. Sci. Lett.*, 223, 427-441.

678

679 Hayward, N., Watts, A. B., Westbrook, G.K. and J. Collier, 1999. A seismic reflection and
680 GLORIA study of compressional deformation in the Gorringe Bank, eastern North Atlantic.
681 *Geophys. J. Int.*, 138, 831-850.

682

683 Jiménez-Munt, M., Fernandez, M., Torné, M. and P. Bird, 2001. The transition from linear
684 to diffuse plate boundary in the Azores-Gibraltar region: results from a thin sheet model.
685 *Earth Planet. Sci. Lett.*, 192, 175-189.

686

687 Lin, A.T. and A.B. Watts, 2002. Origin of the West Taiwan basin by orogenic loading and
688 flexure of a rifted continental margin. *J. Geophys. Res.*, 107, doi: 10.1029/2001JB000669.

689

690 Luis, J.F., 2007. Mirone: A multi-purpose tool for exploring grid data. *Computers &*
691 *Geosciences*, 33, 31-41.

692

693 Maggi, A., Jackson, J., McKenzie, D. and K. Priestley, 2000. Earthquake focal depth,
694 effective elastic thickness and the strength of the continental lithosphere. *Geology*, 28 (6),
695 495– 498.

696

697 Maldonado, A., Somoza, L. and L. Pallares, 1999. The Betic orogen and the Iberian-
698 African boundary in the Gulf of Cadiz: geological evolution (central North Atlantic).
699 Marine Geology, 155 (1-2), 9-43.

700

701 Matias, L., 1996. A sismologia experimental na modelação da estrutura da crosta em
702 Portugal Continental. Tese de Doutoramento. Universidade de Lisboa, Lisboa, 397 pp.

703

704 Medialdea, T., Vegas, R., Somoza, L., Vazquez, J.T., Maldonado, A., Diaz-del Rio, V.,
705 Maestro, A., Córdoba, D. and M. C. Fernandes-Puga, 2004. Structure and evolution of the
706 "Olistostrome" complex of the Gibraltar Arc in the Gulf of Cádiz (eastern Central Atlantic):
707 evidence from two long seismic cross-sections. Marine Geology, 209 (1-4), 173-198.

708

709 Muller, S., Spence, W. and G.L. Choy, 1996. Inelastic models of lithospheric stress – II.
710 Implications for outer-rise seismicity and dynamics. Geophys. J. Int., 125, 54-72.

711

712 Negrodo, A.M., Bird, P., Sanz de Galdeano, C. and E. Buforn, 2002. Neotectonic modeling
713 of the Ibero-Maghrebian region. J. Geophys. Res., 107 (B11), doi:1029/2001JB000743.

714

715 Neves, M.C., Bott, M.H.P. and R.C. Searle, 2004. Patterns of stress at midocean ridges and
716 their offsets due to seafloor subsidence. Tectonophysics, 386 (3-4), 223-242.

717

718 Nocquet, J.M. and E. Calais, 2004. Geodetic Measurements of Crustal Deformation in the
719 Western Mediterranean and Europe. Pure Appl. Geophys., 161, 661-681.

720

721 Okaya, N., Cloetingh, S. and St. Mueller, 1996. A lithospheric cross-section through the
722 Swiss Alps-II. Constraints on the mechanical structure of a continent-continent collision
723 zone. *Geophys. J. Int.*, 127, 399-414.

724

725 Pérez-Gussinyé, M. and T. J. Reston. 2001. Rheological evolution during extension at
726 nonvolcanic rifted margins: Onset of serpentinization and development of detachments
727 leading to continental breakup. *J. Geophys. Res.*, 106, 3961-3975.

728

729 Pinheiro, L. M., Wilson, R., Pena dos Reis, R., Whitmarsh, R.B. and A. Ribeiro, 1996. The
730 Western Iberia Margin: a Geophysical and Geological Overview. *Proceedings of the Ocean
731 Drilling Program, Scientific Results in Whitmarsh, R. B., Sawyer, D. S., Klaus, A. and
732 D.G. Masson, College Station, TX (Ocean Drilling Program), 149, 3-23.*

733

734 Purdy, G.M., 1975. The Eastern end of the Azores-Gibraltar plate boundary. *Geophys. J.R.
735 Astron. Soc.*, 43, 973–1000.

736

737 Ranalli, G., 1995. *Rheology of the Earth*, 2nd ed. Chapman & Hall, London.

738

739 Ranalli, G., 2003. How soft is the crust?. *Tectonophysics*, 361 (3-4), 319-320.

740

741 Sartori, R., Torelli, L., Zitellini, N., Peis, D. and E. Lodolo, 1994. Eastern segment of the
742 Azores-Gibraltar line (central-eastern Atlantic): an oceanic plate boundary with diffuse
743 compressional deformation. *Geology*, 22, 555-558.

744

745 Sibson, R.H., 1974. Frictional constraints on thrust, wrench and normal faults. *Nature*, 249,
746 542-544.

747

748 Stich, D., Serpelloni, E., Mancilla, F.-L. and J. Morales, 2006. Kinematics of the Iberia–
749 Maghreb plate contact from seismic moment tensors and GPS observations.
750 *Tectonophysics*, 426, 295-317.

751

752 Tassara, A., Swain, C., Hackney, R. and J. Kirby, 2007. Elastic thickness structure of South
753 America estimated using wavelets and satellite-derived gravity data. *Earth and Planet. Sci.*
754 *Lett.*, 253, 17-36.

755

756 Terrinha, P., Pinheiro, L. M., Henriot, J.-P., Matias, L., Ivanov, M. K., Monteiro, J. H.,
757 Akhmetzhanov, A., Volkonskaya, A., Cunha, T., Shaskin, P. and M. Rovere, 2003.
758 Tsunamigenic-seismogenic structures, neotectonics, sedimentary processes and slope
759 instability on the southwest Portuguese Margin. *Marine Geology*, 195 (1-4), 55-73.

760

761 Terrinha, P., Matias, L., Vicente, J., Duarte, J., Luís, J., Pinheiro, L., Lourenço, N., Diez,
762 S., Rosas, F., Magalhães, V., Valadares, V., Zitellini, N., Roque, C., Mendes-Víctor, L. and
763 MATESPRO Team, Morphotectonics and Strain Partitioning at the Iberia-Africa plate
764 boundary from multibeam and seismic reflection data, submitted.

765

- 766 Tortella, D., Torné, M. and A. Pérez-Estáun, 1997. Geodynamic Evolution of the Eastern
767 Segment of the Azores-Gibraltar Zone: The Gorringe Bank and the Gulf of Cadiz Region.
768 *Mar. Geophys. Res.*, 19 (3), 211-230.
769
- 770 Udías, A., Lopez Arroyo, A. and J. Mezcuá, 1976. Seismotectonics of the Azores-Alboran
771 region. *Tectonophysics*, 31, 259- 289.
772
- 773 Van Der Beek, P.A. and S. Cloetingh, 1992. Lithospheric flexure and the tectonic evolution
774 of the Betic Cordilleras (SE Spain). *Tectonophysics*, 203 (1-4), 325-344.
775
- 776 Verzhbitsky, E.V. and V.G. Zolotarev, 1989. Heat flow and the Eurasian–African plate
777 boundary in the eastern part of the Azores–Gibraltar fracture zone. *Journal of Geodynamics*
778 11, 267– 273.
779
- 780 Watts, A.B. and J. Stewart, 1998. Gravity anomalies and segmentation of the continental
781 margin offshore West Africa. *Earth and Planet. Sci. Lett.*, 156, 239-252.
782
- 783 Watts, A.B., 2001. *Isostasy and flexure of the lithosphere*. Cambridge University Press,
784 Cambridge.
785
- 786 Watts, A.B. and E. Burov, 2003. Lithospheric strength and its relationship to the elastic and
787 seismogenic layer thickness. *Earth and Planet Sci. Lett.*, 213, 113-131.
788

- 789 Wessel, P. and W.H.F. Smith, 1998. New, improved version of the Generic Mapping Tools
790 Released. EOS Trans. AGU, 79, 579.
791
- 792 Zhang, G.B. and M.H.P. Bott, 2000. Modelling the evolution of asymmetrical basins
793 bounded by high-angle reverse faults with application to foreland basins, Tectonophysics,
794 322 (3), 203-218.
795
- 796 Zitellini, N., Mendes, L.A., Córdoba, D., Danobeitia, J., Nicolich, R., Pellis, R., Ribeiro,
797 A., Sartori, R., Torelli, L., Bartolomé, R., Bortoluzzi, G., Calafato, A., Carrilho, F., Casoni,
798 L., Chierici, F., Corela, C., Correggiari, A., Della Vedova, B., Gràcia, E., Jornet, P.,
799 Landuzzi, M., Ligi, M., Magagnoli, A., Marozzi, G., Matias, L., Penitenti, D., Rodriguez,
800 P., Rovere, M., Terrinha, P., Vigliotti, L. and A. Zahinos Ruiz, 2001. Source of 1755
801 Lisbon Earthquake and Tsunami Investigated. EOS Trans. AGU, 82 (26), 290-291.
802
- 803 Zitellini, N., Rovere, M., Terrinha, P., Chierici, F., Matias, L. and BIGSETS Team, 2004.
804 Neogene through Quaternary tectonic reactivation of SW Iberian passive margin. Pure
805 Appl. Geophys., 161 (3), 565–587.

806

807

808 **Figure Captions**

809

810 Figure 1 – Location map of the study area showing the modelled profile (thick solid line).

811 Shaded relief image of bathymetry and topography from GEBCO digital data

812 (<http://www.ngdc.noaa.gov/mgg/gebco/gebco.html>), with contour interval at 500 m.813 Epicenters for the period 1964-2007 taken from the ISC database (<http://www.isc.ac.uk>)

814 complemented with data from the IM catalogue between 1970-2000. Focal mechanisms are

815 from Carrilho (2005) and the CMT Harvard database

816 (<http://www.seismology.harvard.edu/projects/CMT/>). Structural domains, in decreasing

817 grey intensity from E to W are the Offshore Betic-Rifean domain, the central domain and

818 the Oceanic domain taken from Medialdea et al.(2004). Faults traced after Terrinha et al.

819 (submitted); GqF: Guadalquivir fault, HsF: Horseshoe fault, SVF: S. Vicent Fault, MPF:

820 Marquês de Pombal fault, PSF: Pereira de Sousa fault, GB: Gorringe Bank, CP: Coral

821 Patch. The modelled profile is divided in four zones (oceanic, transition 1, transition 2 and

822 continental) according to the crustal structure and seismicity distribution (in Figure 2 and

823 Figure 3 respectively).

824

825 Figure 2 – Structure of the crust along the profile studied by Fernandez et al. (2004)

826 showing also the extent of the IAM3 profile. P- wave velocities are in km/s and densities in

827 kg/m^3 . OC: oceanic crust, TC: transitional crust, UC: upper continental crust, MC: middle

828 continental crust, LC: lower continental crust. The profile is divided in four zones

829 according to the seismicity distribution (in figure 3).

830

831 Figure 3 – Cross-section showing the vertical seismicity distribution along the modelled
832 profile. The light grey region displays the crustal geometry, without sediments, after the
833 subtraction of the seawater-depth. The focal depths of the earthquakes that fall within a 75
834 km wide window in either side of the profile are projected on the cross-section. Events with
835 magnitude greater than 4 are displayed as larger grey circles. Four different zones are
836 distinguished: a practically aseismic oceanic domain, transition zone 2 dominated by large
837 earthquakes in the Horseshoe Abyssal Plain (see Figure 1), transition zone 1 dominated by
838 small magnitude earthquakes clustering at the base of the crust, and the continental domain
839 characterised by an essentially aseismic mantle inland of Cape St. Vincent (at km 0).

840

841 Figure 4 – Cross-section showing the calculated strength envelopes in compression for
842 selected sites along the profile and the estimated temperature field contoured at a 400°C
843 isotherm interval. **A.** Present-day strength and temperature distribution. The GT1 to GT5
844 indicate the location of the geotherms used to estimate the temperature structure (see text).
845 **B.** An hypothetical thermal scenario and the corresponding strength profiles used to
846 evaluate the effect of the temperature on the modelling results. This scenario may represent
847 an early stage of the Algarve's margin rifting. A cosine bell function was used to
848 interpolate the temperature between geotherm T1 (10 Ma oceanic lithosphere) and T2
849 (present-day continental geotherm).

850

851 Figure 5 –Loads applied to the numerical model. **A.** The dashed line represents the weight
852 of the sediment layer. The solid line is the sum of the water and sediment loads applied at

853 the surface as direct nodal forces. **B.** Restored cross section of the crystalline crust. The
854 water and sediment layers were removed and all density interfaces shifted upwards. **C.** The
855 density anomalies that generate internal gravitational body forces are obtained by
856 subtracting the reference-depth density profile (see text) from the density structure shown
857 above.

858

859 Figure 6 – The deflection of the top surface of the model in response to the topographic and
860 internal gravitational loads (dotted black line) fits the wavelengths (> 150 km) of the
861 bathymetry supported by flexure (grey solid line). The solid dark grey line is the actual
862 bathymetry referenced to the depth of the ocean basin at the SW end of the profile.

863

864 Figure 7 – Close up of the modelling results in the Ocean-Continent Transition zone and
865 adjacent region. Top two panels: stress difference distribution predicted for hypothetical
866 (Figure 4b) and the present-day (Figure 4a) thermal states. Bottom two panels:
867 corresponding density of strain energy. The focal depths of the earthquakes are also plotted
868 for the actual state.

869

870 Figure 8 – Dependence of the strain energy distribution on composition. Top: the
871 composition of the crust is uniform (wet quartzite). Bottom: the crust has a layered
872 composition (as in Figure 2 and Table 1). The present-day thermal structure is assumed in
873 both cases. The strain energy (U) scale is the same as in Figure 7.

874

875 Figure 9 – Estimates of the integrated strength (solid line) along the ocean-continent
876 transition, based on the strength envelopes in compression shown at selected sites. The

877 depth distribution of the modelled stress-difference in the actual state (track at km-150 and
878 km-50) is shown in dark grey for comparison with the strength envelopes. Above ~30 km
879 depth the stress difference is compressive and below is tensile.

Accepted Manuscript

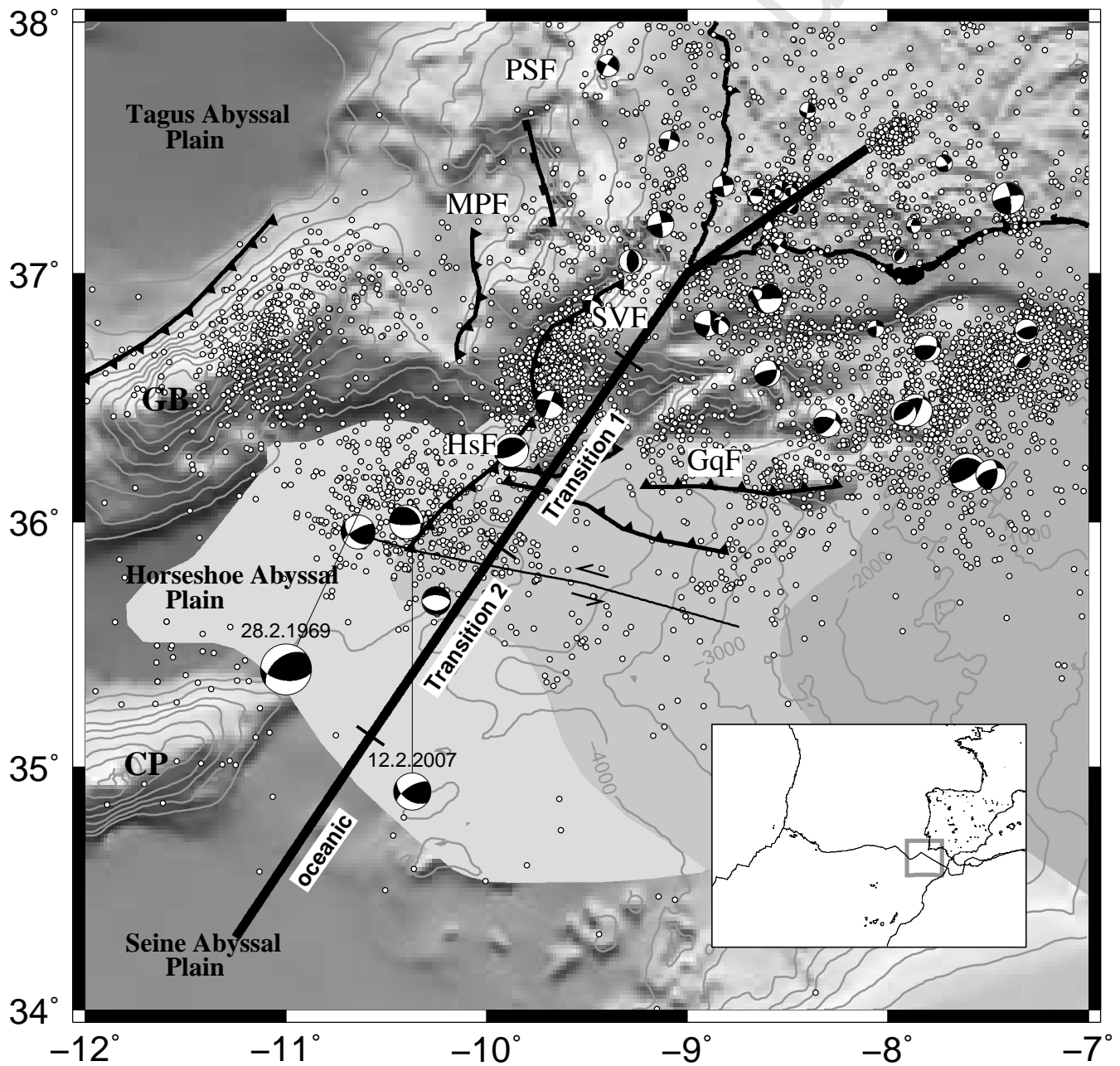
Table 1. Thermal and mechanical material parameters

	Sediments	UCC (wet quartzite)	MCC (wet felsic granulite)	LCC (wet mafic granulite)	OC (wet diabase)	TC (wet quartzite)	Mantle (wet peridotite)
Q [$\mu\text{W m}^{-3}$]	1.2	1.4	0.4	0.4	-	0.4	0.006
K [$\text{W m}^{-1} \text{K}^{-1}$]	2.3	2.5	2.1	2.1	-	2.1	3.0
ρ [kg m^{-3}]	2400	2740	2800	2950	2840	2800	3300
A [$\text{MPa}^{-n} \text{s}^{-1}$]	-	3.2×10^{-4}	8.0×10^{-3}	1.4×10^4	2.0×10^{-4}	3.2×10^{-4}	2.0×10^3
B [kJ mol^{-1}]	-	154	243	445	260	154	471
n	-	2.3	3.1	4.2	3.4	2.3	4.0
E [Pa]	-	0.7×10^{11}	0.7×10^{11}	0.7×10^{11}	0.7×10^{11}	0.7×10^{11}	0.7×10^{11}
ν	-	0.25	0.25	0.25	0.25	0.25	0.25

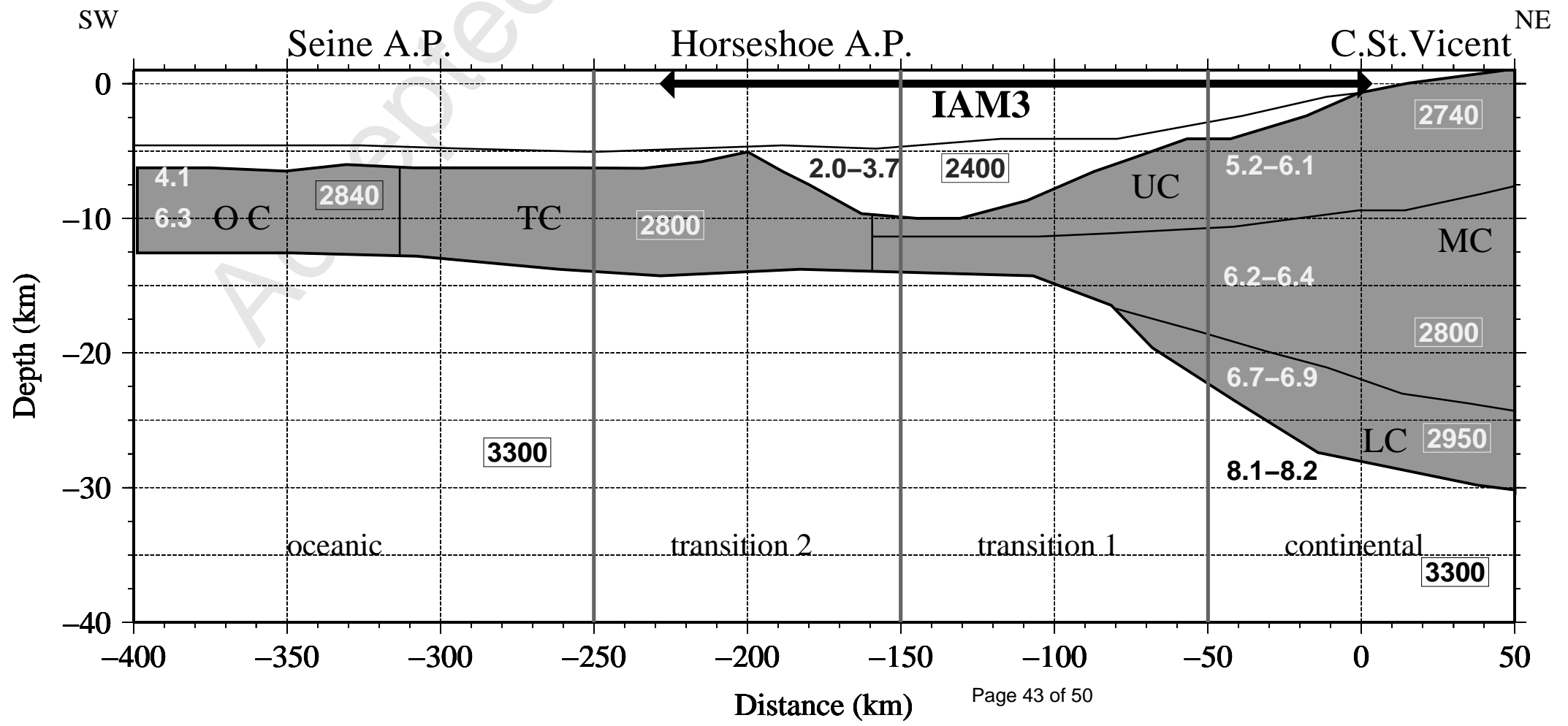
Q:volumetric heat production rate; K:thermal conductivity; ρ :density;A,E,n:material creep parameters;E:Young's modulus; ν :Poisson's ratio
Data from Afonso and Ranalli (2004) and Fernandez et al. (2004).

Accepted Manuscript

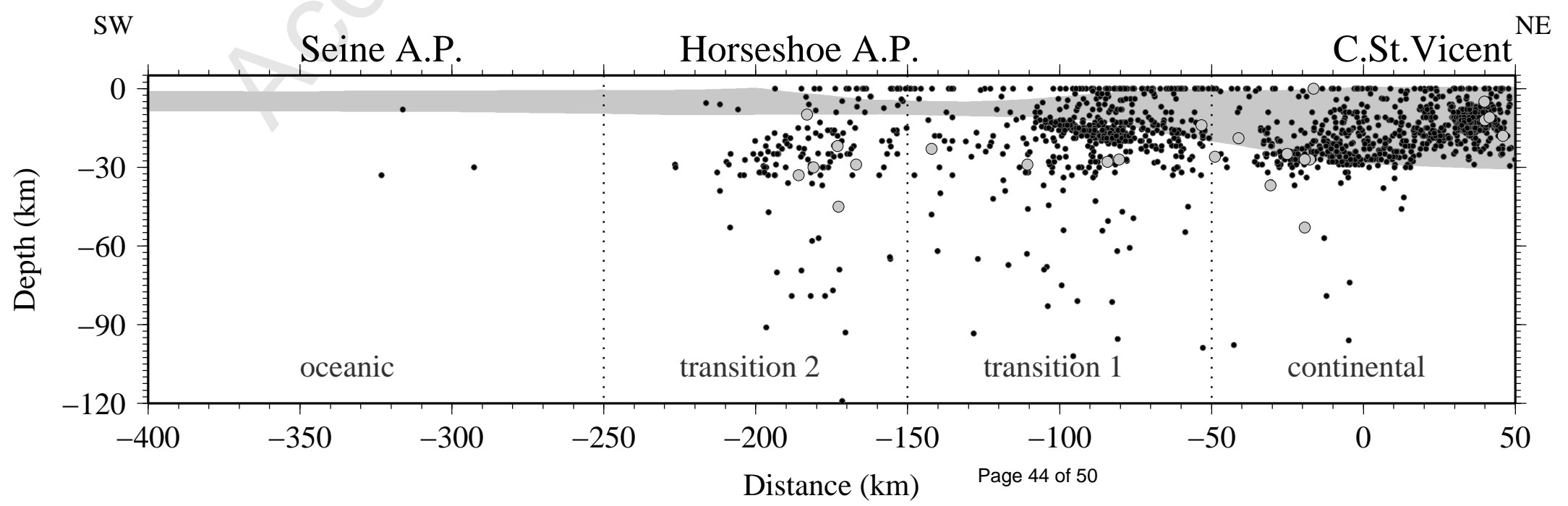
(Neves) Figure 1

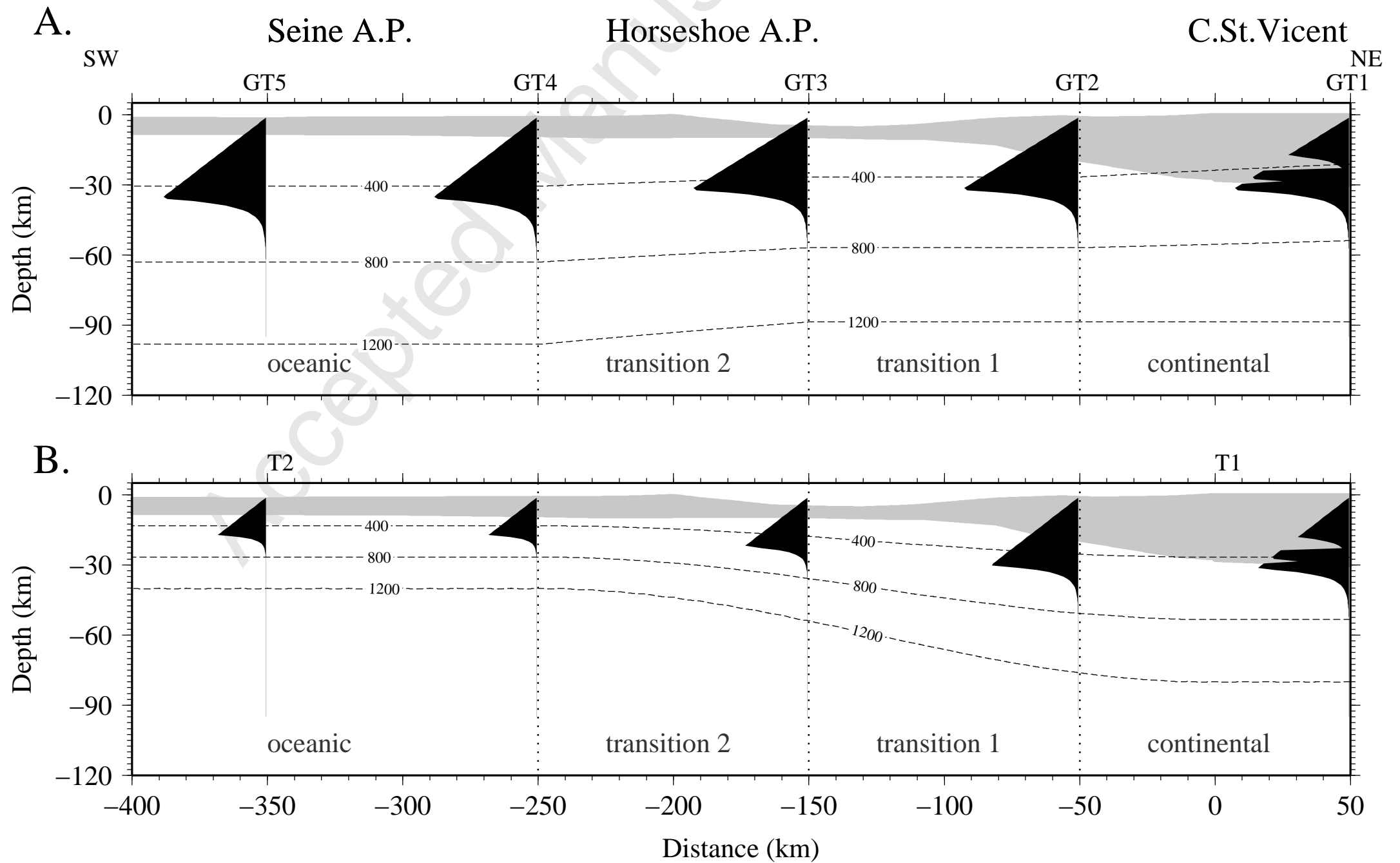


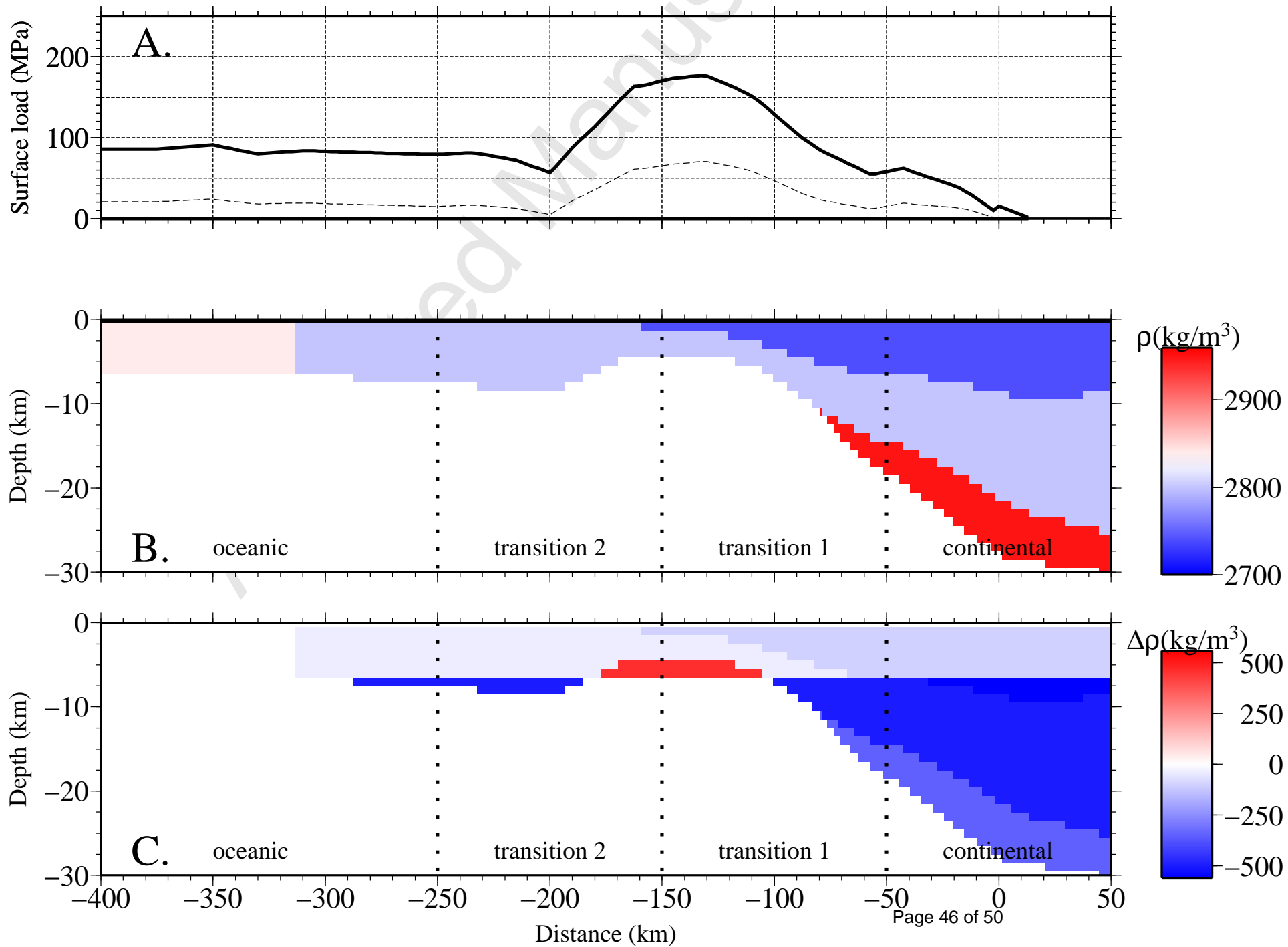
(Neves) Figure 2



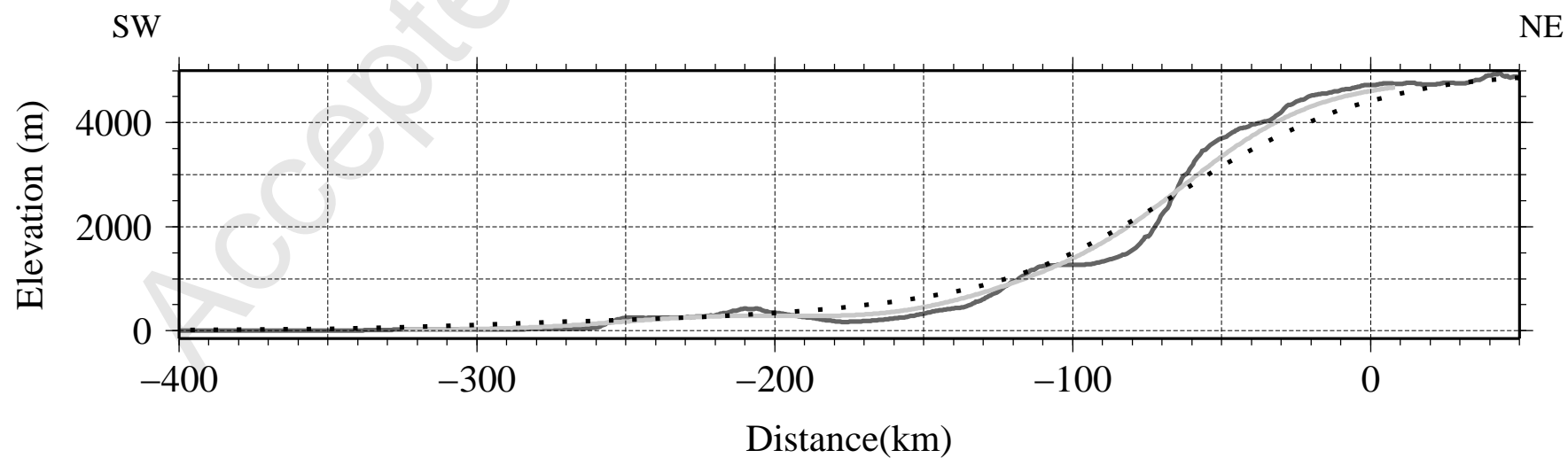
(Neves) Figure 3



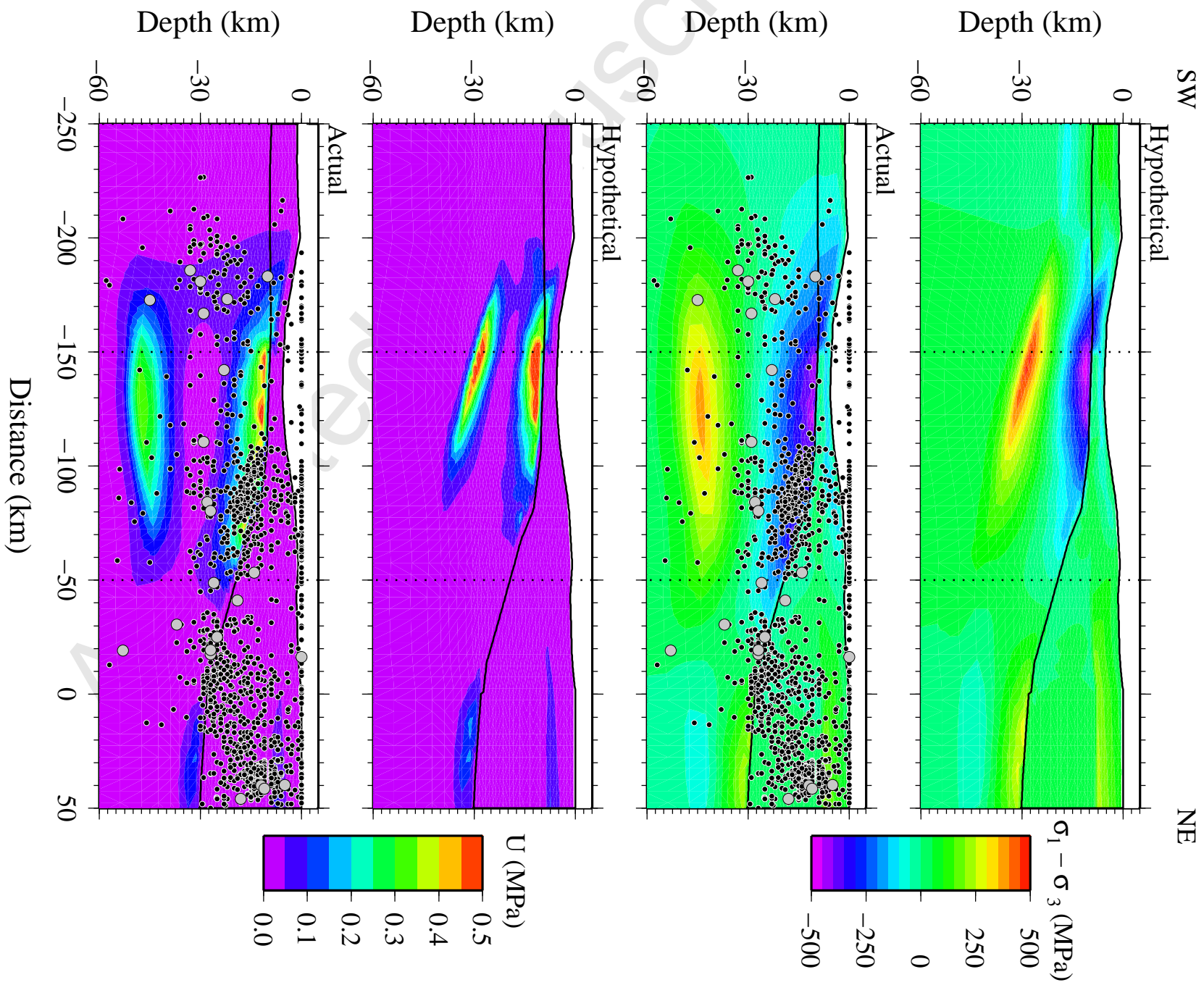




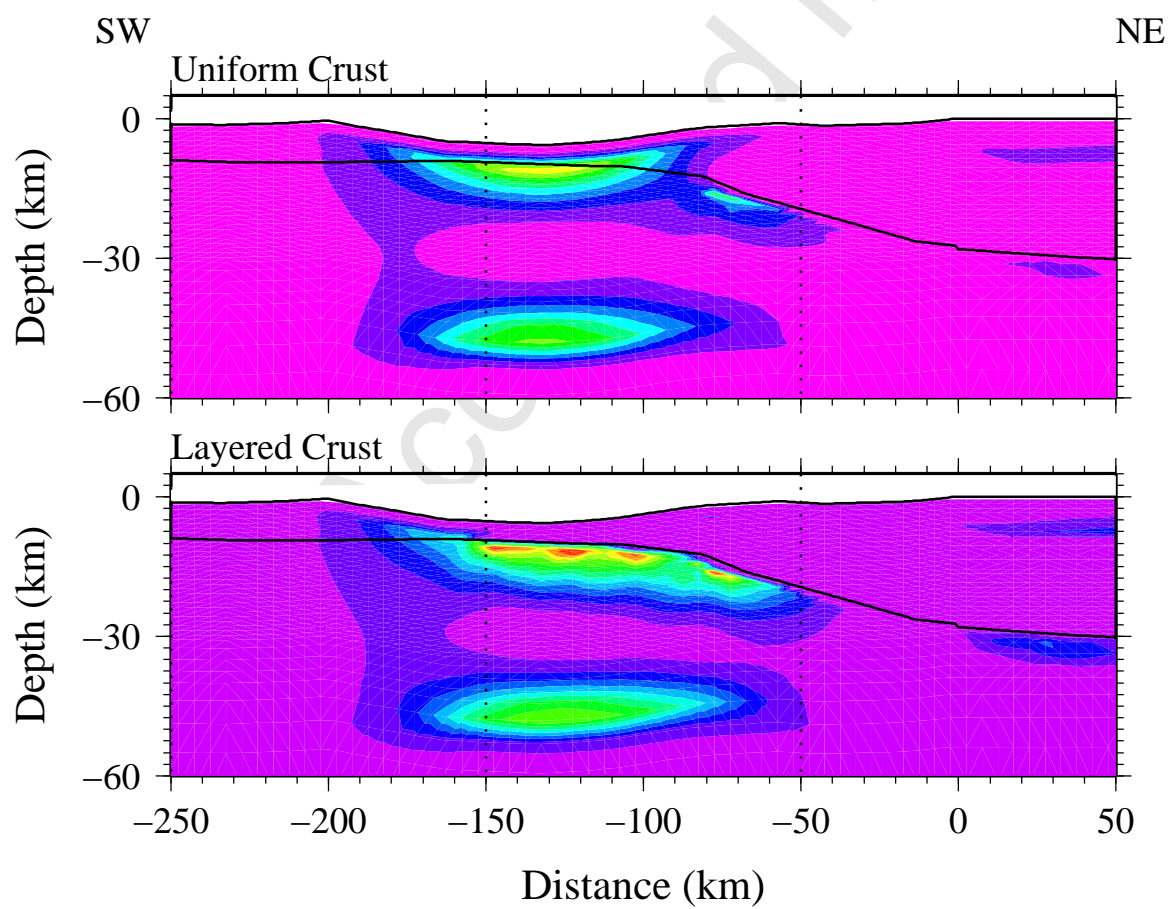
(Neves) Figure 6



(Neves) Figure 7



(Neves) Figure 8



(Neves) Figure 9

